



A helical LC3-interacting region mediates the interaction between the retroviral restriction factor Trim5 α and mammalian autophagy-related ATG8 proteins

Received for publication, May 29, 2018, and in revised form, September 10, 2018. Published, Papers in Press, October 3, 2018, DOI 10.1074/jbc.RA118.004202

✉ Jeremy R. Keown^{#1}, Moyra M. Black[‡], Aaron Ferron[§], Melvyn Yap[§], Michael J. Barnett[‡], ✉ F. Grant Pearce[¶], Jonathan P. Stoye[§], and ✉ David C. Goldstone^{#||2}

From the [‡]School of Biological Sciences, University of Auckland, Auckland 1010, New Zealand, the [§]Francis Crick Institute, London NW1 1ST, United Kingdom, the [¶]School of Biological Sciences, University of Canterbury, Christchurch 8041, New Zealand, and the ^{||}Maurice Wilkins Centre for Molecular Biodiscovery, Auckland 1010, New Zealand

Edited by Norma M. Allewell

The retroviral restriction factor tripartite motif–containing 5 α (Trim5 α) acts during the early postentry stages of the retroviral life cycle to block infection by a broad range of retroviruses, disrupting reverse transcription and integration. The mechanism of this restriction is poorly understood, but it has recently been suggested to involve recruitment of components of the autophagy machinery, including members of the mammalian autophagy-related 8 (ATG8) family involved in targeting proteins to the autophagosome. To better understand the molecular details of this interaction, here we utilized analytical ultracentrifugation to characterize the binding of six ATG8 isoforms and determined the crystal structure of the Trim5 α Bbox coiled-coil region in complex with one member of the mammalian ATG8 proteins, autophagy-related protein LC3B (LC3B). We found that Trim5 α binds all mammalian ATG8s and that, unlike the typical LC3-interacting region (LIR) that binds to mammalian ATG8s through a β -strand motif comprising approximately six residues, LC3B binds to Trim5 α via the α -helical coiled-coil region. The orientation of the structure demonstrated that LC3B could be accommodated within a Trim5 α assembly that can bind the retroviral capsid. However, mutation of the binding interface does not affect retroviral restriction. Comparison of the typical linear β -strand LIR with our atypical helical LIR reveals a conservation of the presentation of residues that are required for the interaction with LC3B. This observation expands the range of LC3B-binding proteins to include helical binding motifs and

demonstrates a link between Trim5 α and components of the autophagosome.

The ATG8-like proteins are essential for expansion of the phagophore membrane and mediate targeting and assembly of protein complexes to the autophagosome (1). The six mammalian ATG8 (mATG8)³ isoforms (LC3A, LC3B, LC3C, GABARAP, GABARAPL1, and GABARAPL2) are orthologues of the *Saccharomyces cerevisiae* ATG8 protein and share a conserved sequence and structure. Structurally, the mATG8s consist of a β -grasp fold that is shared with ubiquitin and ubiquitin-like proteins (2). In addition, mATG8s have two further helices at the N terminus that complete the fold. A conjugation pathway similar to the ubiquitin conjugation system results in the proteins being C-terminally lipidated with phosphatidylethanolamine, providing an anchor to the autophagosomal membrane. As key components of selective autophagy, they can act to target specific proteins to the autophagosome together with proteins and organelles targeted for destruction within the autophagosome.

The mATG8s bind target proteins through a conserved LC3-interacting region (LIR) (3). The mATG8s, and their interaction with the LIR motif, has been well-characterized by structural biology (2, 4–6). The typical LIR motif is formed by a large hydrophobic residue and a small hydrophobic residue separated by two intervening amino acids that are not arginine, glycine, proline, or lysine. It is often accompanied by an acidic residue at the N-terminal end of the motif giving the following prosite (7) motif annotation [DEST][WFY]-{RGKP}{RGKP}-[ILV]. Upon binding, the LIR motif forms an extended β -strand that extends the central β -sheet packing parallel to strand β 2. Similarly a GABARAP-interacting motif has recently been described where a small hydrophobic residue is located immediately following the large hydrophobic residue (8). The large and small hydrophobic residues of the LIR are accommodated within two hydrophobic pockets located on the surface of the

This work was supported by a Rutherford Discovery Fellowship from the New Zealand government administered by the Royal Society of New Zealand (to D. C. G.) and a Royal Society of New Zealand Marsden Grant (to D. C. G.). This work was also supported in part by the Francis Crick Institute, which receives its core funding from Cancer Research UK Grant FC001162, United Kingdom Medical Research Council Grant FC001162, and Wellcome Trust Grant FC001162 (to A. F., M. Y., and J. P. S.). The authors declare that they have no conflicts of interest with the contents of this article.

✂ Author's Choice—Final version open access under the terms of the Creative Commons CC-BY license.

This article contains Figs. S1–S4.

The atomic coordinates and structure factors (code 5W9A) have been deposited in the Protein Data Bank (<http://www.pdb.org/>).

¹ Present address: Division of Structural Biology, University of Oxford, Oxford OX3 7BN, United Kingdom.

² To whom correspondence should be addressed: School of Biological Sciences, University of Auckland, Auckland 1010, New Zealand. Tel.: 649-923-4607; E-mail: d.goldstone@auckland.ac.nz.

³ The abbreviations used are: mATG8, mammalian ATG8; LIR, LC3-interacting region; SV-AUC, sedimentation velocity analytical ultracentrifugation; PDB, Protein Data Bank; SEC-MALLS, size-exclusion chromatography coupled to multiangle laser light scattering; TCEP, tris-(2-carboxyethyl) phosphine hydrochloride.

ATG8 protein (2) The first pocket, often termed the W pocket, accommodates the large hydrophobic residue, and the second pocket, often termed the L pocket, accommodates the small hydrophobic residue.

Recently, several studies have described a link between members of the TRIM (tripartite motif–containing) protein family and autophagy (9–13). Members of the TRIM protein family are characterized by a conserved N-terminal domain architecture consisting of a RING domain, which confers E3 ubiquitin ligase activity; one or two Bbox domains; and a coiled-coil region (14). The C-terminal domain of TRIM proteins is varied with a PRY/SPRY domain being the most common (15). The coiled-coil region assembles as an elongated anti-parallel dimer placing the RING and Bbox domains from each monomer at opposite ends of the coiled-coil, separating them by ~ 160 Å (16–18). Family members act in many cellular pathways, with approximately one-third implicated in innate immunity (19–22). One of the most studied family members is the antiretroviral postentry restriction factor Trim5 α .

Trim5 α acts during early stages of the retroviral life cycle to prevent retroviral infection, disrupting reverse transcription and integration of the virus. The restriction of a particular virus requires recognition of the intact lattice of capsid protein that forms the inner shell of the retrovirus (23, 24). Recognition of the incoming virus is mediated by the C-terminal domain PRY/SPRY domain. A set of variable loops in the PRY/SPRY domain dictates the subset of viruses that the Trim5 α of different species is able to restrict (25).

Trim5 α blocks infection during at least two stages of the retroviral life cycle. The first block, prior to reverse transcription, is contingent on the ubiquitin-proteasome system and results in premature disassembly of the capsid core and release of viral proteins and RNA (26). Inhibition of the proteasome or disruption of the Trim5 α RING domain prevents Trim5 α from blocking reverse transcription but does not rescue infection, indicating the presence of a second block to infection (27, 28).

In 2014 Mandell *et al.* (9) used a siRNA screen to show that a large number of TRIM proteins alter the number of LC3B puncta in cells, suggesting a role in regulating autophagy. In these experiments Trim5 α was proposed to act as a selective autophagy receptor, targeting a restricted virus to the autophagosome for degradation. Furthermore, using co-immunoprecipitation they demonstrated potential interactions with components of the autophagic machinery including ULK1, beclin1, sequestosome1/p62, and members of the mATG8 family.

To investigate the interaction between Trim5 α and components of the autophagy machinery, we have undertaken *in vitro* experiments, using purified proteins, to examine the interaction between members of the mammalian ATG8 family and the coiled-coil region of Trim5 α . We have demonstrated a direct interaction and determined the strength and stoichiometry of this interaction. Furthermore, we have crystallized the complex between Trim5 α and LC3B. Our structure demonstrates that a cryptic LIR is located in the Trim5 α coiled-coil α -helix and that an LIR need not be present as a β -strand or disordered region of the protein. Although retroviral infection assays demonstrate that the interaction is not required for restriction of HIV-1, this structure demonstrates an expanded range of binding sites for

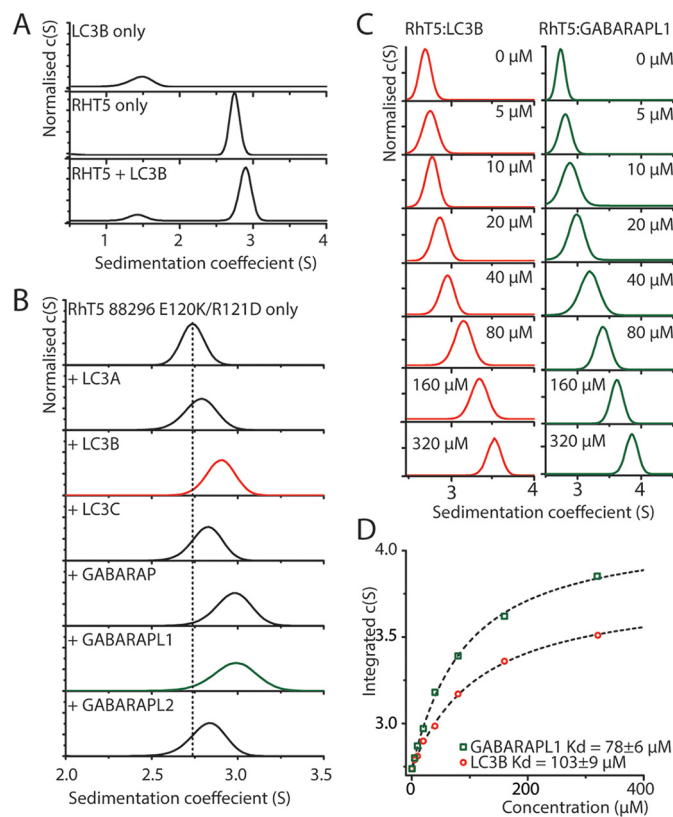


Figure 1. SV-AUC analysis shows that purified Trim5 α binds to six isoforms of mATG8s. A, c(s) analysis of SV-AUC of 20 μ M LC3B, RHT5 88–296 EK/RD, or an equimolar mixture. B, c(s) analysis of 20 μ M of RHT5 88–296 EK/RD and equimolar concentration of the six mATG8 isoforms. C, c(s) analysis of 20 μ M RHT5 88–296 EK/RD and increasing concentrations (0–320 μ M) of either LC3B or GABARAPL1. D, peak centroid position derived from integration of the c(s) function from C versus LC3B or GABARAPL1 concentration. A one-site binding model has been used to determine the equilibrium dissociation constant (dashed lines).

LC3B and members of the mammalian ATG8 proteins and provides a structural link between Trim5 α and components of the autophagosome.

Results

Trim5 α binds directly to the six mammalian ATG8 isoforms

The interaction between mATG8 family members and Trim5 α was identified by co-immunoprecipitation studies (9). Further peptide array experiments then mapped binding to regions of the Trim5 α coiled-coil domain. This suggests an atypical interaction, because ATG8 proteins usually bind an LIR motif found in a β -strand or unstructured loop. To address this discrepancy, we sought to reproduce the interaction with purified components.

To do this, we utilized a construct of Trim5 α from Rhesus macaque encompassing the Bbox coiled-coil regions with an E120K/R121D mutation (RHT5 88–296 EK/RD) that blocks the higher-order assembly of the protein (16, 29), and LC3B expressed in *Escherichia coli*. Our initial small-scale pulldown experiments failed to recapitulate the interaction. Therefore, we employed sedimentation velocity analytical ultracentrifugation (SV-AUC) to examine the interaction between the Trim5 α coiled-coil and LC3B where the two components were closer to equilibrium conditions. Analysis was undertaken

Trim5 α binds to LC3B via a helical LIR motif

using the continuous distribution of sedimentation coefficients function, $c(s)$, for each component alone and an equimolar mixture of RhT5 88–296 EK/RD and LC3B (Fig. 1A). The $c(s)$ distribution for RhT5 88–296 EK/RD and LC3B showed symmetric peaks with sedimentation coefficients of 2.74 S ($S_{20,w}$ 2.86 S) and 1.56 S ($S_{20,w}$ 1.7 S), respectively, consistent with RhT5 88–296 EK/RD being a dimer and LC3B being a monomer. Analysis of the mixture showed a slow-moving peak at 1.56 S corresponding to free LC3B and a fast-moving peak at 2.90 S. This peak is at a greater S value than that seen for RhT5 88–296 EK/RD alone and represents the unresolved co-sedimentation of both the RhT5 88–296 EK/RD and the 88–296 EK/RD+LC3B complex components. Because no peak was observed for free RhT5 88–296 EK/RD, this suggests that the interaction is under fast exchange in solution relative to the time of sedimentation (30).

To determine whether the interaction with Trim5 α is common to all mATG8s, we undertook further sedimentation velocity experiments employing RhT5 88–296 EK/RD and LC3A, LC3C, GABARAP, GABARAPL1, and GABARAPL2 and analyzed the effect on the position of the fast-moving peak. In each case the addition of a mATG8 resulted in an increase in the apparent sedimentation coefficient in the integrated $c(s)$ of the RhT5 88–296 EK/RD peak. Based upon the magnitude of the change in the peak position, that likely corresponds to the strength of the interaction, the rank order of affinity was GABARAPL1 followed by GABARAP, LC3B, GABARAPL2, and LC3C, with LC3A being the weakest (Fig. 1B).

To measure the affinity of the interaction, two representative mATG8 proteins, LC3B and GABARAPL1, were chosen and titrated (0–320 μ M) against a 20 μ M RhT5 88–296 EK/RD and analyzed binding by SV–AUC. In both the LC3B and GABARAPL1 titrations, a concentration-dependent shift was observed for the fast-moving species with the S value of the peak increasing as the concentration of either protein was increased. To determine the affinity of the interaction, the S value of the faster moving peak in the $c(s)$ distribution was integrated and plotted against the ATG8 protein concentration. The curve was then fit to a single site-binding model. The equilibrium dissociation constant (K_D) determined in this manner was 103 ± 9 and 78 ± 6 μ M for LC3B and GABARAPL1, respectively (Fig. 1, C and D).

LC3B binds directly to the Trim5 α coiled-coil via helical LIR motif

To identify the site of interaction of mATG8s within the Trim5 α coiled-coil, we undertook crystallization experiments employing RhT5 88–296 EK/RD and all the mATG8s. Crystals of a complex between RhT5 88–296 EK/RD and LC3B were obtained and harvested for X-ray diffraction analysis. The crystals diffracted anisotropically to a resolution of 4.11–2.74 Å and belong to the space group P2₁2₁. The structure was determined by molecular replacement using the structure of the Bbox coiled-coil region of Trim5 α (PDB code 4TN3) and LC3B (PDB code 3WAO) as search models. The structure was refined to a final R/R_{free} of 25.9%/27.4%, respectively. Two copies of RhT5 88–296 EK/RD and two copies of LC3B are present in the asymmetric unit (full data collection and model refinement sta-

Table 1
Data collection and refinement statistics

The statistics for the highest resolution shell are shown in parentheses.

	RhT5 88–296 E120K/R121D: LC3B 2–119
Data collection statistics	
Diffraction source	MX2 Beamline, Australian Synchrotron
Space group	P 2 21 21
Unit cell dimensions	
a, b, c (Å)	72.01, 115.32, 174.16
α, β, γ (°)	90, 90, 90
Resolution range (Å)	40.73–2.74 (2.97–2.74)
Ellipsoidal resolution (Å) (direction) ^{a,b}	2.723 (a*) 2.768 (b*) 4.111 (c*)
Total no. of reflections (ellipsoidal) ^a	298,683 (16,041)
No. of unique reflections (ellipsoidal) ^a	24,308 (1215)
Average multiplicity ^a	12.3 (13.2)
Completeness (%) (ellipsoidal) ^a	92.9 (61.7)
$I/\sigma < I >$ (ellipsoidal) ^a	13.0 (1.5)
R_{meas}	0.121 (1.91)
R_{pim}	0.047 (0.719)
$CC_{1/2}$ ^a	1 (0.367)
Wilson B factor	83.71
Refinement statistics	
R_{work}	0.259
R_{free}	0.274
Number of nonhydrogen atoms	4849
Macromolecules	4845
Ligand (zinc)	4
Protein residues	611
RMS	
Bonds	0.002
Angles	0.43
Ramachandran (%)	
Favored	96.8
Allowed	3.2
Outliers	0
Rotamer outliers (%)	1.2
Clashscore	5.5
Average B-factor	86.3
Macromolecules	86.3
Ligand (zinc)	95.6
PDB accession code	5W9A

^a These statistics are for data that were truncated by STARANISO to remove poorly measured reflections affected by anisotropy.

^b The resolution limits are shown for each of the three reciprocal lattice axes (a*, b*, and c*). STARANISO has applied an approximately elliptical cutoff to the reflection data.

istics are presented in Table 1). The final model comprises residues 95–288 of RhT5 and residues 88–296 and 4–117 of LC3B.

The two RhT5 88–296 EK/RD monomers are arranged as an elongated antiparallel dimer as seen previously (Fig. 2A). Comparison of the refined model with our previous structure of the Trim5 α Bbox and coiled-coil reveals a high degree of structural similarity with an root-mean-square deviation of 1.1 Å across equivalent C α atoms (Fig. S1). There is no evidence of flexibility in the coiled-coil between this model and the previously determined structure as was observed when comparing other structures of Trim protein coiled-coils (17, 18).

The two LC3B molecules adopt the typical ubiquitin-like fold and are highly similar to previously determined structures (root-mean-square deviation 0.9 Å to PDB code 2LUE) (Fig. S1). Within the crystal they are positioned toward the center and on either side of the Trim5 α coiled-coil. Each LC3B monomer makes essentially identical interactions with a single RhT5 88–296 EK/RD monomer with no interactions between the two LC3B molecules.

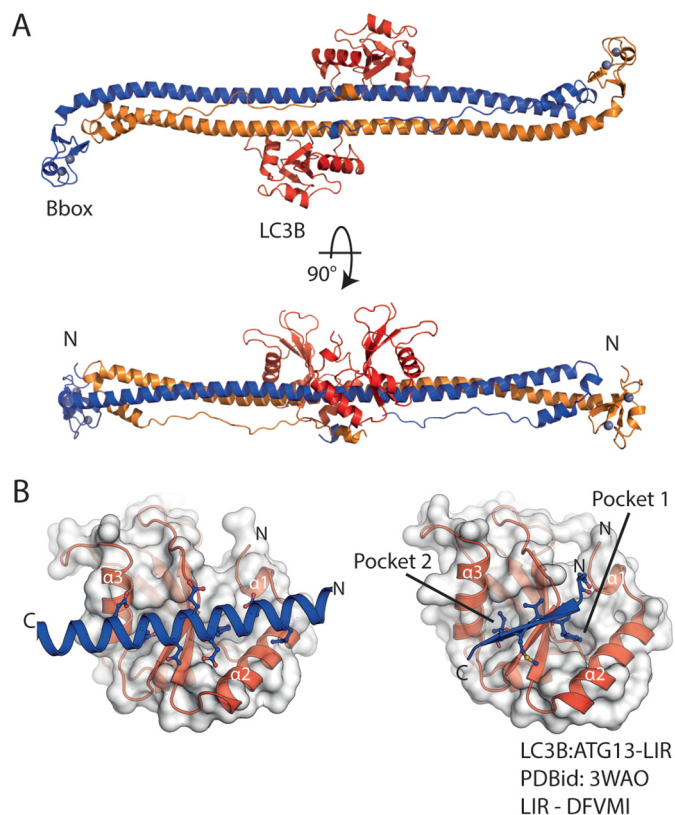


Figure 2. The coiled coil of Trim5 α binds LC3B through a helical motif. A, cartoon representation of the RhT5 88–296 EK/RD-LC3B protein complex. Chain A/B (blue/orange) form the Trim5 α antiparallel coiled coil dimer, LC3B molecules are red, and zinc atoms are shown as spheres (silver). B, expanded view of the LC3B-binding site (left) and comparison with a typical β -strand LIR motif (LC3B-ATG13-LIR PDB code 3WAO). Both the helical and β -strand LIR occupy and proceed in the same orientation through the LC3B-binding site.

At the interface, the bound section of the long Trim5 α helix occupies the same groove on the LC3B surface that is used by a typical LIR interaction. Moreover, it is presented in same orientation running parallel with strand β 2 of from LC3B (Fig. 2B). The Trim5 α -LC3B interface buries $\sim 825 \text{ \AA}^2$ of surface area of each molecule, corresponding to 5% of the RhT5 88–295 EK/RD surface area and 11% of the LC3B surface area. An electrostatic surface calculation (Fig. S2) shows an area of strong negative charge located in the center of the Trim5 α coiled coil that is complementary to the general positive charge of the LC3B surface. Residues involved in the interaction span the residue range of Gln¹⁸⁹-Glu²¹⁰ in Trim5 α .

As seen for a typical LIR motif, the interaction centers around Trim5 α side-chain interactions in the large hydrophobic pocket of LC3B. Here, it is the side chain of Trim5 α Trp¹⁹⁶ that protrudes away from the coiled coil and occupies the large hydrophobic pocket of LC3B. By contrast, the second hydrophobic pocket that is typically occupied by a small hydrophobic residue is unoccupied in our structure. Instead, the side chain of Gln²⁰³ is located above the pocket with the side chain amide making a hydrogen bond with the backbone carboxyl of Leu⁵³ in strand β 2 of LC3B.

In addition, there are further interactions outside the hydrophobic pockets that are mediated by acidic residues on the Trim5 α coiled-coil. Glu¹⁹² forms a salt bridge with Lys⁵¹ on

strand β 2 of LC3B, Glu¹⁹⁷ forms a hydrogen bond with His²⁷ at the C terminus of helix α 2 from LC3B, and Glu²⁰⁶ forms potential salt bridges with Arg⁶⁹ and Arg⁷⁰ at the C terminus of helix α 3 (Fig. 3). Further interactions are mediated by Ser¹⁹⁹ that makes a hydrogen bond with the backbone carboxyl of Lys⁵¹ and the side-chain amine of Gln¹⁸⁹ that makes a hydrogen bond with the side chain of Asp¹⁹ on helix α 2 of LC3B.

Mutational analysis of the Trim5 α -LC3B interface

To investigate the importance of specific residues in the Trim5 α -LC3B interface, we undertook site-directed mutagenesis to probe the contribution of key residues in the interface and assessed complex formation by SV-AUC. In all assays LC3B and mutants of RhT5 88–296 EK/RD were mixed at an equal concentration of 20 μM . The effects of mutations were judged based upon the magnitude of the perturbation to the fast moving peak corresponding to the Trim-LC3B complex in the $c(s)$ analysis. Control size-exclusion chromatography coupled to multiangle laser light scattering (SEC-MALLS) and $c(s)$ analysis of all Trim5 α mutants alone demonstrate that they retain the dimeric assembly and do not show large perturbations of the overall structure of the protein (Fig. S3 and Fig. 4, B and C, black lines).

The Trp¹⁹⁶ side chain is at the center of the interface filling the large hydrophobic pocket of LC3B. The effect of mutating this residue to alanine was assessed for binding to each of the six mATG8 isoforms. Analysis by the $c(s)$ distribution showed that mutation of Trp¹⁹⁶ to alanine abolished binding between the LC3A, LC3B, LC3C, and GABARAPL2, whereas GABARAP and GABARAPL1 still bound but with a reduced affinity (Fig. 4A). This suggests that although Trp¹⁹⁶ was important for the affinity of binding, other residues in the interface are able to maintain the interaction in its absence. To test this hypothesis we probed the role of other Trim5 α residues in the interface by mutating them to either an alanine or lysine. Each mutant was assayed against LC3B and GABARAPL1 because these two mATG8s showed the greatest affinity for WT Trim5 α .

We first tested residues likely to contribute to the acidic surface charge at the center of the Trim5 α coiled coil. Mutations of both Glu¹⁹² and Glu²⁰⁶, that make charge-charge interactions in the interface, to either alanine or lysine disrupt binding to LC3B with the lysine mutation showing the anticipated stronger effect (Fig. 4, B and C). In GABARAPL1 the alanine mutations have little effect, whereas the E192K lysine disrupts binding the E206K mutation has minimal effect. Mutation of Glu¹⁹⁷ to alanine, removing the interaction with Gln²⁶/His²⁷, reduced the binding of LC3B but did not abolish it completely. However, the mutation had no effect on the binding of GABARAPL1. A charge swapping mutation of E198K creating repulsion against Lys⁵¹ reduced binding against LC3B and GABARAPL1. These mutations demonstrate that the general electrostatic interaction contributes to binding.

In addition to the ionic interactions, three hydrogen bond contacts that contribute to the interface were also identified. Therefore, these interactions were also probed by mutating the residue on Trim5 α to alanine. Mutation of Gln¹⁸⁹, which forms a hydrogen bond to Asp¹⁹ in LC3B, had a minimal effect on LC3B binding. However, this mutation resulted in an increase

Trim5 α binds to LC3B via a helical LIR motif

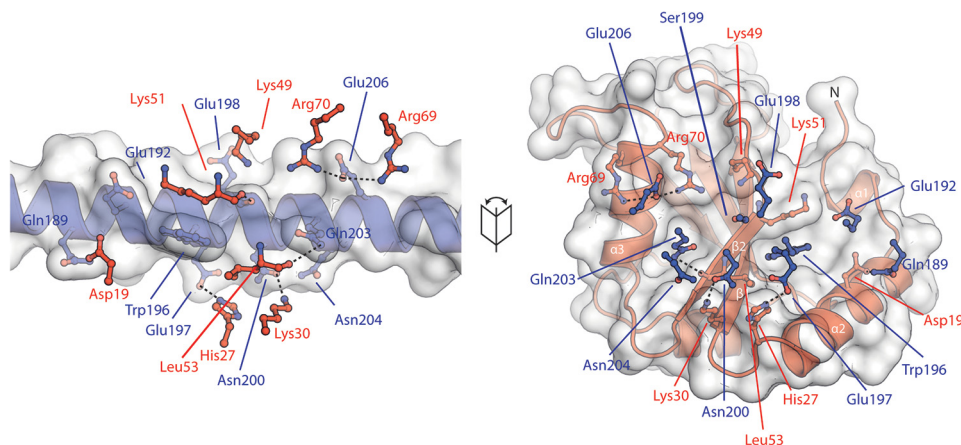


Figure 3. Interactions mediating binding of LC3B to the Trim5 α coiled coil. A fold out of the LC3B–RhT5 α interaction with RhT5 α in blue and LC3B in red is shown. Residues from the opposing molecule are shown as ball-and-stick representation with potential hydrogen bonds as dashed lines. Trp¹⁹⁶ of Trim5 α occupies pocket 1 of LC3B.

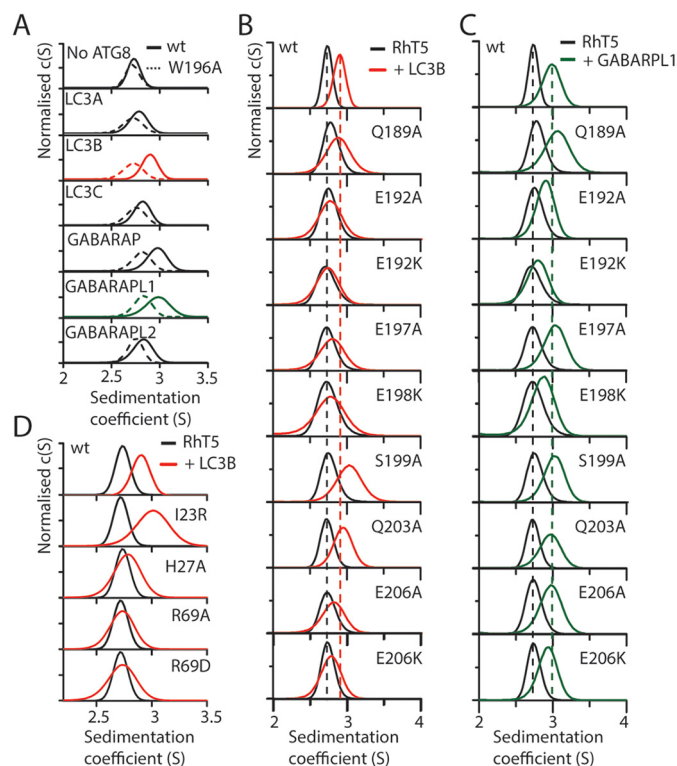


Figure 4. Mutational analysis of the LC3B–RhT5 α interface. A, *c(s)* analysis of the RhT5 88–296 EK/RD–mATG8 interaction with all mATG8 proteins at 20 μ M equimolar concentration, WT (solid lines), and W196A RhT5 88–296 EK/RD (dashed lines). B and C, *c(s)* analysis of mixtures of WT and mutant RhT5 88–296 EK/RD with either LC3B (B) or GABARAPL1 (C). Dashed lines indicate the position of RhT5 88–296 EK/RD (black) or with the addition of either LC3B (red) or GABARAPL1 (green). D, *c(s)* analysis of LC3B mutants (red) mixed with WT RhT5 88–296 EK/RD (black).

in the *S* value of the fast moving peak for GABARAPL1 binding, suggesting a stronger interaction. Structure comparison of GABARAPL1 with LC3B shows a glutamate at position 19 (compared with the aspartate in LC3B), which would likely clash with Gln¹⁸⁹. Therefore, the observed increase in GABARAPL1 binding may result from the alanine substitution relieving this clash.

In a similar manner, mutation of Gln²⁰³ to alanine was found to increase the affinity of binding to LC3B but did not affect

binding to GABARAPL1. Gln²⁰³ is located at the edge of the small hydrophobic pocket and forms a hydrogen bond with the backbone of Leu⁵³. Mutation to alanine would remove this hydrogen bond and was predicted to weaken and not strengthen the interaction. However, it may be that the loss of a hydrogen bond is compensated for by accommodation of the alanine residue in the previously unoccupied L pocket on LC3B.

In addition to interface residues in the Trim5 α coiled coil, we identified three residues on LC3B that were probed by mutagenesis for their contribution to the binding of Trim5 α . Mutation of LC3B His²⁷ to alanine removes a hydrogen bond formed with Glu¹⁹⁷ on Trim5 α and has the similar effect to the RhT5 E197A mutant (Fig. 4D). Substitution of LC3B Arg⁶⁹ with either alanine or aspartate is predicted to disrupt ionic interactions with Glu²¹⁰ and Glu²⁰⁶ of Trim5 α and abolished binding. In the large hydrophobic pocket, Ile²³ is packed adjacent to Trp¹⁹⁶ of Trim5 α . Mutation to an arginine was predicted to occlude binding into this pocket by filling the same space as occupied by the tryptophan side chain. Surprisingly, this mutation resulted in a faster moving peak in the SV–AUC analysis, suggesting a stronger interaction. However, given the guanidinium head group of arginine residues can pack in a π -stacking conformation with aromatic side chains, this mode of interaction with Trp¹⁹⁶ provides a possible explanation for the observed increase in binding.

Previous studies have demonstrated an interaction between Trim5 α and components of the autophagy machinery, including members of the ATG family. Furthermore microscopy experiments have demonstrated co-localization of Trim5 α in autophagic structures in cells (31). The role of autophagy in restriction is less clear with conflicting results reported (9, 12, 31). To assess whether the interaction with the mATG8s play a key role in the restriction of retroviral infection, we undertook restriction assays to examine the effect of W196A and E197A mutations on restriction by either Trim5 α or TrimCyp. The inclusion of either mutation individually or the double mutant had no effect on the infectivity of HIV-1 in our restriction assay (Table 2). Both Trim5 α and TrimCyp exhibit a secondary block to infection in the presence of the proteasome inhibitor

Table 2**Restriction assay of Trim5 and TrimCyp mutants in the presence and absence of proteasome inhibitor MG132**

The cells were transduced with vectors expressing YFP and either TRIM5, TRIMCyp, or their mutants before challenging with HIV-1 expressing GFP, in the presence or absence of MG132. The cells were analyzed by flow cytometry 48 h after challenge. The numbers are ratios of percentages of infected cells containing restriction factor to percentages of infected cells that do not contain restriction factor.

	Without MG132	1 μ g/ml MG132	16 μ g/ml MG132
Trim 5 α	0.12 \pm 0.06	0.14 \pm 0.04	0.12 \pm 0.01
Trim 5 α W196A/E197A	0.10 \pm 0.05	0.11 \pm 0.05	0.09 \pm 0.03
Trim 5 α E197A	0.12 \pm 0.03	0.12 \pm 0.04	0.19 \pm 0.03
TrimCypA	0.10 \pm 0.06	0.10 \pm 0.02	0.09 \pm 0.02
TrimCypA W196A	0.08 \pm 0.03	0.08 \pm 0.05	0.05 \pm 0.03
TrimCypA W196A/E197A	0.10 \pm 0.06	0.11 \pm 0.07	0.05 \pm 0.01
TrimCypA E197A	0.12 \pm 0.05	0.13 \pm 0.08	0.11 \pm 0.03

MG132. This block occurs after the completion of reverse transcription but prior to integration of the provirus. The inclusion of proteasome inhibitor at either 1 or 16 μ g/ml had no effect on the infectivity of virus in our assay. These results are in agreement with those published by Imam *et al.* (31). This suggests that although Trim5 α is able to bind LC3B and members of the mammalian ATG8 family, they do not contribute to the restriction of retroviral infection at either the primary block prior to reverse transcription or the secondary block after reverse transcription.

Discussion

During autophagy members of the mATG8 family play a crucial role in phagophore formation and expansion. Modification of LC3B, and other mATG8s, via cleavage of the C terminus and the subsequent conjugation of a phosphatidylethanolamine lipid to the C terminus, is a key marker of autophagosome formation. This modification anchors the mATG8s to the autophagosome where they act as an adaptor, tethering substrate proteins, including components of the autophagosome maturation pathway and selective autophagy receptors, to the autophagosomal membrane.

Previously characterized interactions between ATG8 proteins and their binding partners show a conserved mode of interaction (3) comprising a linear binding motif with the consensus sequence of [DEST][WFY]-{RGKP}{RGKP}-[ILV] arranged as a β -strand with the large and small hydrophobic residues located in pockets on the surface of the ATG8 protein. The structure now presented here demonstrates a second mode of binding where a helical motif occupies the same binding groove on the surface of LC3B with the large hydrophobic pocket similarly occupied.

Based upon our structural observations and biophysical characterization of this interaction we propose a "helical LIR" motif, where upon accounting for the difference in residue spacing imposed by the helical secondary structure an equivalent consensus sequence is accommodated. This new motif would have a consensus sequence of an acidic residue with a three-amino acid spacer N-terminal to the large aromatic amino acid and then a further six amino acids N-terminal to the residue that occupies the small hydrophobic pocket ([DEST]-X₃-[WFY]-X₆-[LIVQ]). This results in key residues being presented along a single face of an α -helix. In the case of Trim5 α the residues Glu¹⁹², Trp¹⁹⁶, and Gln²⁰³ fulfill these positions,

with Gln²⁰³ located on the edge of the small hydrophobic pocket. Mutation of these residues alters binding, either decreasing the affinity or in the case of Gln²⁰³ substitution with a small hydrophobic residues results in an increase in binding. Although these residues are located in key positions in the binding groove, our data demonstrate that other residues present on the helix contribute to binding. This is consistent with the increased surface area and number of residues presented by the helix, 10 residues burying \sim 820 \AA^2 compared with 5 amino acids burying \sim 610 \AA^2 for a typical LIR motif. Furthermore, mutation of residues in the helical LIR contribute differently to binding of LC3B and GABARAP1, suggesting subtle differences in the recognition of different ATG8 proteins.

To examine further features that contribute to the LC3B-binding site, we aligned the coiled-coil region of Trim5 α from 57 species with unique sequences present in the UniProt database (Fig. S4). It is evident that although there are conserved residues that we have shown contributing to binding, other amino acids are less well-conserved. Of note, Trp¹⁹⁶ is not strictly conserved across the Trim5 α of all species. Mapping sequences to an evolutionary tree, we observe a clear sequence division at this position between the new- and old-world monkeys. This divergence maps to after the separation between the new- and old-world monkeys that occurred during the Oligocene era, between 30 and 40 million years ago and prior to the divergence of the apes and old-world monkeys \sim 10–20 million years ago (32), suggesting that a tryptophan at this position has been acquired and retained.

Based upon previously determined structures of the Trim5 α PRY/SPRY domain (33, 34) and an overlap with residues in the L2 linker region that are present in structures of both the PRY/SPRY domain (34) and the Bbox coiled-coil region of Trim5 α (16), it is possible to construct a model of the Trim5 α molecule that positions the SPRY domain from each monomer adjacent to one another at the center of the coiled-coil region (16, 35–37). This model positions the variable loops of the SPRY domain to recognize the retroviral capsid, and the Bbox and RING domains are available for higher-order assembly and ubiquitylation. Inclusion of LC3B into this model using our current structure (Fig. 5) now positions the LC3B either side of the center of the coiled-coil, adjacent to the SPRY domains, without interfering with the positioning of the SPRY domains or making interactions with regions of the L2. Further examination of the orientation of the LC3B relative to the SPRY domain positions the C termini of the LC3Bs on the opposite side of the coiled coil. This demonstrates that LC3B could be accommodated within the Trim5 α higher-order assembly and would allow the SPRY domain to remain accessible to recognize substrates, whereas lipidated LC3B could tether Trim5 α to the autophagosomal membrane.

Comparison of the affinity of interaction of the helical LIR with that of the typical LIR–LC3B interactions suggests that the LC3B–Trim5 α interaction is at the lower end of reported affinities, with typical interaction in the K_D range of 1–50 μ M range (38). However, because both LC3B molecules present in our model are oriented with the C terminus exposed, we would expect a single Trim5 α dimer to bind two LC3B molecules. With LC3B tethered on the autophagosomal membrane, this

Trim5 α binds to LC3B via a helical LIR motif

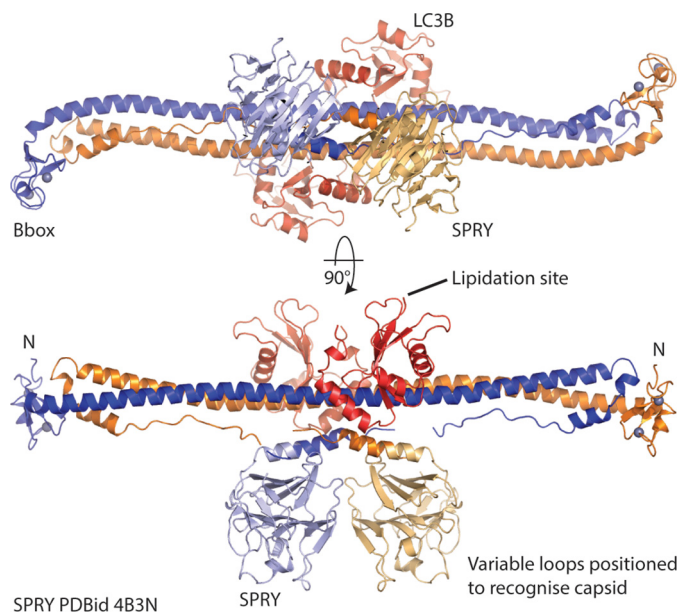


Figure 5. Model of Trim5 α -LC3B complex. The SPRY domains from Rhesus Trim5 α (PDB code 4B3N) are positioned on the Trim5 α Bbox coiled coil (PDB code 4TN3) by superposition of common residues. The structure of the RhT5 α -LC3B complex (this work) was then superimposed on 4TN3 to position the LC3B molecules. This model positions the variable loops of the SPRY domain to recognize capsid, whereas the lipidation site at the C terminus of LC3B is available to be incorporated in the autophagosomal membrane.

would generate an avid interaction and greatly amplify the strength of binding.

Members of the TRIM protein family have an emerging role in autophagy. The structure presented here provides the first molecular insight into the interaction of TRIM proteins with components of the autophagy machinery. This interaction proceeds through a helical motif and alters the current paradigm of binding to members of the ATG8 protein family.

Experimental procedures

Protein purification

Mammalian ATG8 and Trim5 α constructs were inserted into pET47 and expressed with an N-terminal His tag in *E. coli* LOBSTR BL21(DE3) cells. The proteins were purified by immobilized nickel-affinity chromatography, and the His tag was removed by incubation with HRV 3C protease prior to anion exchange (6 ml of Resource Q) and size-exclusion chromatography using a Superdex 200 (16/60) column equilibrated with 10 mM Tris/HCl, pH 7.8, 150 mM NaCl, 0.1 mM TCEP. Proteins were concentrated to 20 mg/ml using Vivaspinn concentrators and stored at -80°C until required.

Analytical ultracentrifugation

All sedimentation velocity analytical ultracentrifugation experiments were carried out at 20°C (293 K) using a Beckman Coulter model XL-I with absorbance optics in double sector charcoal filled Epon center pieces. All samples were centrifuged in a Beckman Coulter eight-hole An-50 Ti rotor at 50,000 rpm. Prior to the experiments all samples were exhaustively dialyzed against a buffer containing 10 mM

Tris/HCl, pH 8, 150 mM NaCl, and 0.1 mM TCEP. SEDNTERP (39) was used to determine a solvent density of 1.005 g ml^{-1} and a viscosity of 0.01021 cp. The data were analyzed using a continuous $c(s)$ distribution in SEDFIT (39). Because many experiments contained mixtures of two proteins, each with a unique partial specific volume, a constant value of 0.73 ml g^{-1} was used for all samples.

Crystallization and structure determination

The Trim5 α construct RhT5 88–296 E120K/R121D and LC3B construct 2–119 were mixed at equimolar concentrations ($330\text{ }\mu\text{M}$) and crystallized by the vapor diffusion method at 290 K. The protein mixture was combined with a precipitant mixture containing 0.2 M NH_4Cl , 0.1 M Tris/HCl, pH 8, 20% PEG 6,000 at a ratio of 1:1 and allowed to equilibrate. Large plate crystals formed over a period of $\sim 48\text{ h}$.

The crystals were harvested into a cryoprotectant containing the precipitant mixture supplemented with 20% glycerol and flash-frozen in liquid nitrogen. Diffraction experiments were conducted at the Australian synchrotron. The data were collected at 9900 eV.

The data were indexed with XDS (40), and initial merging and scaling with AIMLESS (41) indicated significant anisotropy in the strength of diffraction. Thus an anisotropic resolution cutoff was applied to the data by the STARANISO server (Global Phasing Limited) giving a maximum resolution of $2.74\text{ }\text{\AA}$. The structure was then determined by molecular replacement in PHASER (42) using the Trim5 α dimer (PDB code 4TN3) and a single LC3B molecule (PDB code 3WAO) as search models. The second LC3B molecule was generated by noncrystallographic symmetry, rotating the model 180° and aligning based on the Trim5 α dimer. The model was then completed using iterative rounds of manual model building in COOT (43) and refinement in PHENIX (44). The data collection and refinement statistics are presented in Table 1.

SEC-MALLS

SEC-MALLS was used to determine the molecular weight and oligomeric state of RhT5 88–296 EK/RD and LC3B mutants. Samples ($100\text{ }\mu\text{l}$) were applied to a Superdex 75 Increase 10/300 column in a running buffer containing 10 mM Tris/HCl, pH 7.8, 150 mM NaCl, 0.1 mM TCEP, and 3 mM azide. The MALLS unit comprised a Dionex HPLC with a PSS SLD7000 7-angle MALLS detector and a Shodex RI-101 differential refractive index detector. The data were analyzed using the PSS winGPC Unichrom software package.

Restriction assays

CRFK cells were transduced with vectors expressing YFP and either TRIM5, TRIMCyp, or their mutants before challenging with HIV-1 expressing GFP, in the presence or absence of either $1\text{ }\mu\text{g/ml}$ MG132 or $16\text{ }\mu\text{g/ml}$ MG132. The cells were analyzed by flow cytometry 48 h after challenge. The numbers are ratios of percentages of infected cells containing restriction factor to percentages of infected cells that do not contain restriction factor. A ratio of less than 0.3 was taken to indicate restriction (45).

Author contributions—J. R. K. and D. C. G. conceptualization; J. R. K. and D. C. G. formal analysis; J. R. K., M. M. B., A. F., M. W. Y., M. J. B., F. G. P., and J. P. S. investigation; J. R. K., M. W. Y., J. P. S., and D. C. G. writing-original draft; J. R. K. and D. C. G. writing-review and editing; F. G. P. resources; J. P. S. supervision.

Acknowledgments—Plasmids encoding LC3A-C and GABARAP proteins used for subcloning were a kind gift from Prof. Ren Dobson (University of Canterbury). We acknowledge the New Zealand Synchrotron group for access to the MX Beamlines at the Australian Synchrotron. Access to analytical ultracentrifuge facilities was supported by funds from the Maurice Wilkins Centre for Molecular Biodiscovery (to D. C. G.), a Centre of Research Excellence funded by the New Zealand government.

References

- Nakatogawa, H., Ichimura, Y., and Ohsumi, Y. (2007) Atg8, a ubiquitin-like protein required for autophagosome formation, mediates membrane tethering and hemifusion. *Cell* **130**, 165–178 [CrossRef Medline](#)
- Popelka, H., and Klionsky, D. J. (2015) Analysis of the native conformation of the LIR/AIM motif in the Atg8/LC3/GABARAP-binding proteins. *Autophagy* **11**, 2153–2159 [CrossRef Medline](#)
- Birgisdottir, Á. B., Lamark, T., and Johansen, T. (2013) The LIR motif: crucial for selective autophagy. *J. Cell Sci.* **126**, 3237–3247 [Medline](#)
- Suzuki, H., Tabata, K., Morita, E., Kawasaki, M., Kato, R., Dobson, R. C., Yoshimori, T., and Wakatsuki, S. (2014) Structural basis of the autophagy-related LC3/Atg13 LIR complex: recognition and interaction mechanism. *Structure* **22**, 47–58 [CrossRef Medline](#)
- McEwan, D. G., Popovic, D., Gubas, A., Terawaki, S., Suzuki, H., Stadel, D., Coxon, F. P., Miranda de Stegmann, D., Bhogaraju, S., Maddi, K., Gatti, E., Helfrich, M. H., Wakatsuki, S., Behrends, C., Pierre, P., et al. (2015) PLEKHM1 regulates autophagosome-lysosome fusion through HOPS complex and LC3/GABARAP proteins. *Mol. Cell* **57**, 39–54 [CrossRef Medline](#)
- Klionsky, D. J., and Schulman, B. A. (2014) Dynamic regulation of macroautophagy by distinctive ubiquitin-like proteins. *Nat. Struct. Mol. Biol.* **21**, 336–345 [CrossRef Medline](#)
- Sigrist, C. J., de Castro, E., Cerutti, L., Cucho, B. A., Hulo, N., Bridge, A., Bougueleret, L., and Xenarios, I. (2013) New and continuing developments at PROSITE. *Nucleic Acids Res.* **41**, D344–D347 [Medline](#)
- Rogov, V. V., Stolz, A., Ravichandran, A. C., Rios-Szwed, D. O., Suzuki, H., Kniss, A., Löhr, F., Wakatsuki, S., Dötsch, V., Dikic, I., Dobson, R. C., and McEwan, D. G. (2017) Structural and functional analysis of the GABARAP interaction motif (GIM). *EMBO Rep.* **18**, 1382–1396 [CrossRef Medline](#)
- Mandell, M. A., Jain, A., Arko-Mensah, J., Chauhan, S., Kimura, T., Dinkins, C., Silvestri, G., Münch, J., Kirchhoff, F., Simonsen, A., Wei, Y., Levine, B., Johansen, T., and Deretic, V. (2014) TRIM proteins regulate autophagy and can target autophagic substrates by direct recognition. *Dev. Cell* **30**, 394–409 [CrossRef Medline](#)
- Kimura, T., Mandell, M., and Deretic, V. (2016) Precision autophagy directed by receptor regulators: emerging examples within the TRIM family. *J. Cell Sci.* **129**, 881–891 [CrossRef Medline](#)
- Mandell, M. A., Kimura, T., Jain, A., Johansen, T., and Deretic, V. (2014) TRIM proteins regulate autophagy: TRIM5 is a selective autophagy receptor mediating HIV-1 restriction. *Autophagy* **10**, 2387–2388 [CrossRef Medline](#)
- Ribeiro, C. M., Sarrami-Forooshani, R., Setiawan, L. C., Zijlstra-Willems, E. M., van Hamme, J. L., Tigchelaar, W., van der Wel, N. N., Kootstra, N. A., Gringhuis, S. I., and Geijtenbeek, T. B. (2016) Receptor usage dictates HIV-1 restriction by human TRIM5 α in dendritic cell subsets. *Nature* **540**, 448–452 [CrossRef Medline](#)
- Chauhan, S., Kumar, S., Jain, A., Ponpuak, M., Mudd, M. H., Kimura, T., Choi, S. W., Peters, R., Mandell, M., Bruun, J.-A., Johansen, T., and Deretic, V. (2016) TRIMs and galectins globally cooperate and TRIM16 and galectin-3 co-direct autophagy in endomembrane damage homeostasis. *Dev. Cell* **39**, 13–27 [CrossRef Medline](#)
- Reymond, A., Meroni, G., Fantozzi, A., Merla, G., Cairo, S., Luzi, L., Riganelli, D., Zanaria, E., Messali, S., Cainarca, S., Guffanti, A., Minucci, S., Pelicci, P. G., and Ballabio, A. (2001) The tripartite motif family identifies cell compartments. *EMBO J.* **20**, 2140–2151 [CrossRef Medline](#)
- Ozato, K., Shin, D.-M., Chang, T.-H., and Morse, H. C., 3rd (2008) TRIM family proteins and their emerging roles in innate immunity. *Nat. Rev. Immunol.* **8**, 849–860 [CrossRef Medline](#)
- Goldstone, D. C., Walker, P. A., Calder, L. J., Coombs, P. J., Kirkpatrick, J., Ball, N. J., Hilditch, L., Yap, M. W., Rosenthal, P. B., Stoye, J. P., and Taylor, I. A. (2014) Structural studies of postentry restriction factors reveal antiparallel dimers that enable avid binding to the HIV-1 capsid lattice. *Proc. Natl. Acad. Sci. U.S.A.* **111**, 9609–9614 [CrossRef Medline](#)
- Sanchez, J. G., Okreglicka, K., Chandrasekaran, V., Welker, J. M., Sundquist, W. I., and Pornillos, O. (2014) The tripartite motif coiled-coil is an elongated antiparallel hairpin dimer. *Proc. Natl. Acad. Sci. U.S.A.* **111**, 2494–2499 [CrossRef Medline](#)
- Weinert, C., Morger, D., Djekic, A., Grütter, M. G., and Mittl, P. R. (2015) Crystal structure of TRIM20 C-terminal coiled-coil/B30.2 fragment: implications for the recognition of higher order oligomers. *Sci. Rep.* **5**, 10819 [CrossRef Medline](#)
- Pertel, T., Hausmann, S., Morger, D., Züger, S., Guerra, J., Lascano, J., Reinhard, C., Santoni, F. A., Uchil, P. D., Chatel, L., Bisiaux, A., Albert, M. L., Strambio-De-Castillia, C., Mothes, W., Pizzato, M., et al. (2011) TRIM5 is an innate immune sensor for the retrovirus capsid lattice. *Nature* **472**, 361–365 [CrossRef Medline](#)
- Uchil, P. D., Hinz, A., Siegel, S., Coenen-Stass, A., Pertel, T., Luban, J., and Mothes, W. (2013) TRIM protein-mediated regulation of inflammatory and innate immune signaling and its association with antiretroviral activity. *J. Virol.* **87**, 257–272 [CrossRef Medline](#)
- Rajsbaum, R., García-Sastre, A., and Versteeg, G. A. (2014) TRIMmunity: the roles of the TRIM E3-ubiquitin ligase family in innate antiviral immunity. *J. Mol. Biol.* **426**, 1265–1284 [CrossRef Medline](#)
- Tareen, S. U., and Emerman, M. (2011) Human Trim5 α has additional activities that are uncoupled from retroviral capsid recognition. *Virology* **409**, 113–120 [CrossRef Medline](#)
- Dodding, M. P., Bock, M., Yap, M. W., and Stoye, J. P. (2005) Capsid processing requirements for abrogation of Fv1 and Ref1 restriction. *J. Virol.* **79**, 10571–10577 [CrossRef Medline](#)
- Forshey, B. M., Shi, J., and Aiken, C. (2005) Structural requirements for recognition of the human immunodeficiency virus type 1 core during host restriction in owl monkey cells. *J. Virol.* **79**, 869–875 [CrossRef Medline](#)
- Ohkura, S., Yap, M. W., Sheldon, T., and Stoye, J. P. (2006) All three variable regions of the TRIM5 α B30.2 domain contribute to the specificity of retrovirus restriction. *J. Virol.* **80**, 8554–8565 [CrossRef Medline](#)
- Kutluay, S. B., Perez-Caballero, D., and Bieniasz, P. D. (2013) Fates of retroviral core components during unrestricted and TRIM5-restricted infection. *PLOS Pathog.* **9**, e1003214 [CrossRef Medline](#)
- Anderson, J. L., Campbell, E. M., Wu, X., Vandegraaff, N., Engelman, A., and Hope, T. J. (2006) Proteasome inhibition reveals that a functional preintegration complex intermediate can be generated during restriction by diverse TRIM5 proteins. *J. Virol.* **80**, 9754–9760 [CrossRef Medline](#)
- Roa, A., Hayashi, F., Yang, Y., Lienlaf, M., Zhou, J., Shi, J., Watanabe, S., Kigawa, T., Yokoyama, S., Aiken, C., and Diaz-Griffero, F. (2012) RING domain mutations uncouple TRIM5 α restriction of HIV-1 from inhibition of reverse transcription and acceleration of uncoating. *J. Virol.* **86**, 1717–1727 [CrossRef Medline](#)
- Keown, J. R., Yang, J. X., Douglas, J., and Goldstone, D. C. (2016) Characterisation of assembly and ubiquitylation by the RBCC motif of Trim5 α . *Sci. Rep.* **6**, 26837 [CrossRef Medline](#)
- Dam, J., and Schuck, P. (2005) Sedimentation velocity analysis of heterogeneous protein-protein interactions: sedimentation coefficient distributions c(s) and asymptotic boundary profiles from Gilbert-Jenkins theory. *Biophys. J.* **89**, 651–666 [CrossRef Medline](#)

Trim5 α binds to LC3B via a helical LIR motif

31. Imam, S., Talley, S., Nelson, R. S., Dharan, A., O'Connor, C., Hope, T. J., and Campbell, E. M. (2016) TRIM5 α degradation via autophagy is not required for retroviral restriction. *J. Virol.* **90**, 3400–3410 [CrossRef Medline](#)
32. Schrago, C. G., and Russo, C. A. (2003) Timing the origin of new world monkeys. *Mol. Biol. Evol.* **20**, 1620–1625 [CrossRef Medline](#)
33. Biris, N., Yang, Y., Taylor, A. B., Tomashevski, A., Guo, M., Hart, P. J., Diaz-Griffero, F., and Ivanov, D. N. (2012) Structure of the rhesus monkey TRIM5 α PRYSPRY domain, the HIV capsid recognition module. *Proc. Natl. Acad. Sci. U.S.A.* **109**, 13278–13283 [CrossRef Medline](#)
34. Yang, H., Ji, X., Zhao, G., Ning, J., Zhao, Q., Aiken, C., Gronenborn, A. M., Zhang, P., and Xiong, Y. (2012) Structural insight into HIV-1 capsid recognition by rhesus TRIM5 α . *Proc. Natl. Acad. Sci. U.S.A.* **109**, 18372–18377 [CrossRef Medline](#)
35. Wagner, J. M., Roganowicz, M. D., Skorupka, K., Alam, S. L., Christensen, D., Doss, G., Wan, Y., Frank, G. A., Ganser-Pornillos, B. K., Sundquist, W. I., and Pornillos, O. (2016) Mechanism of B-box 2 domain-mediated higher-order assembly of the retroviral restriction factor TRIM5 α . *eLife* **5**, e16309 [CrossRef Medline](#)
36. Li, Y.-L., Chandrasekaran, V., Carter, S. D., Woodward, C. L., Christensen, D. E., Dryden, K. A., Pornillos, O., Yeager, M., Ganser-Pornillos, B. K., Jensen, G. J., and Sundquist, W. I. (2016) Primate TRIM5 proteins form hexagonal nets on HIV-1 capsids. *eLife* **5**, e16269 [CrossRef Medline](#)
37. Jia, X., Zhao, Q., and Xiong, Y. (2015) HIV suppression by host restriction factors and viral immune evasion. *Curr. Opin. Struct. Biol.* **31**, 106–114 [CrossRef Medline](#)
38. Zaffagnini, G., and Martens, S. (2016) Mechanisms of selective autophagy. *J. Mol. Biol.* **428**, 1714–1724 [CrossRef Medline](#)
39. Schuck, P. (2000) Size-distribution analysis of macromolecules by sedimentation velocity ultracentrifugation and Lamm equation modeling. *Biophys. J.* **78**, 1606–1619 [CrossRef Medline](#)
40. Kabsch, W. (2010) XDS. *XDS. Acta Crystallogr. D Biol. Crystallogr.* **66**, 125–132 [CrossRef Medline](#)
41. Evans, P. R., and Murshudov, G. N. (2013) How good are my data and what is the resolution? *Acta Crystallogr. D Biol. Crystallogr.* **69**, 1204–1214 [CrossRef Medline](#)
42. McCoy, A. J. (2007) Solving structures of protein complexes by molecular replacement with *Phaser*. *Acta Crystallogr. D Biol. Crystallogr.* **63**, 32–41 [CrossRef Medline](#)
43. Emsley, P., Lohkamp, B., Scott, W. G., and Cowtan, K. (2010) Features and development of *Coot*. *Acta Crystallogr. D Biol. Crystallogr.* **66**, 486–501 [CrossRef Medline](#)
44. Adams, P. D., Baker, D., Brunger, A. T., Das, R., DiMaio, F., Read, R. J., Richardson, D. C., Richardson, J. S., and Terwilliger, T. C. (2013) Advances, interactions, and future developments in the CNS, Phenix, and Rosetta structural biology software systems. *Annu. Rev. Biophys.* **42**, 265–287 [CrossRef Medline](#)
45. Yap, M. W., Dodding, M. P., and Stoye, J. P. (2006) Trim-cyclophilin A fusion proteins can restrict human immunodeficiency virus type 1 infection at two distinct phases in the viral life cycle. *J. Virol.* **80**, 4061–4067 [CrossRef Medline](#)